Operational Forecasts of Cloud Cover and Water Vapour For ESO Observatories:

Maintenance, Revision of the Movement Algorithm and Development of a Transparency Index

Final report
to
European Southern Observatories

by

D. André Erasmus, Ph.D.
(Certified Consulting Meteorologist)

Deneys Maartens and Ruby van Rooyen
(Research Assistants)

30 April, 2003

Purchase Order
65015/ODG/01/8636/CNI/LET

TABLE OF CONTENTS

1. Background

Forecasts of cloud cover and water vapour have been issued routinely since August 1998 for European Southern Observatory (ESO) telescope sites at Paranal and La Silla. The forecasts are generated automatically *via* the running of time-controlled scripts that download the required input data and run the specially developed computer programme that produces the forecast. The forecast products are then posted on a Web page (http://www.eso.org/gen-fac/pubs/astclim/forecast/meteo/ERASMUS/) for user access.

In the first version of the forecast programme the input data consisted of 6.7 μm GOES-8 satellite imagery from the Co-operative Institute for Research in the Atmosphere (CIRA) and upper-air meteorological model data from the European Centre for Medium-Range Forecasting (ECMWF). The use of these data facilitated the observation and forecasting of high altitude cirrus clouds and precipitable water vapour (PWV). A test of the operational use of the first version of the forecast programme was completed in August 1999 (Erasmus and Maartens, 1999). It was demonstrated that the operational forecast system had been successfully commissioned, that the operational forecasts met predetermined forecast accuracy specifications and continuation of the operational forecasts was indicated.

An upgrade of the forecast programme, which involved the additional use of 10.7 μm GOES-8 satellite data and surface weather observations from the telescope sites, was completed in 2001 (Erasmus and Maartens, 2001). In this study it was verified that the addition of the 10.7 μm GOES-8 satellite data improved cloud detection. Improved accuracy in PWV measurement was also achieved by implementing a revision of the GOES-8 UTH calibration coefficients and by using surface measurements. This upgraded version of the forecast programme was put into operational use in April 2001. (A partial upgrade involving the additional use of surface meteorological data was implemented operationally in May 2000.)

In September 2001, continued maintenance of the operational forecast system was proposed. Included in this proposal were a revision of the algorithm that defines cloud and water vapour movement and the development of a satellite-based transparency index. This report presents the results of the work performed to reach these objectives and is divided into the following sections:

(i) maintenance of the operational forecasts (Section 2),
(ii) revision of the movement algorithm (Section 3),
(iii) verification of forecast accuracy (Section 4), and
(iv) a satellite-based transparency index (Section 5).

2. Maintenance of the operational forecasts

Operational forecasts are made automatically *via* the running of time-controlled (cron) UNIX scripts. These scripts check periodically for the availability of new ECMWF model and GOES-8 satellite data, run the forecast programme and update the forecast. Maintenance of the operational forecasts is therefore critically dependent on the timely delivery of the input data from the data providers. Reliability of data delivery and forecast production was checked by monitoring email messages from the ESO Weather Watch service and by analysing the forecast append files at

the operational forecast web site: www.eso.org/gen-fac/pubs/astclim/forecast/meteo/ERASMUS/).

For the maintenance period covered under the purchase order that has reference to this report, namely, 1 July 2001 – 31 December 2002 (548 days), forecasts were issued on 521 days giving a reliability of 95%. For 16 of the 27 days on which forecasts were missed the cause was a breakdown in satellite data delivery from CIRA. A dispute between ESO and CIRA halted satellite data delivery for an additional 8 days. The remaining three days were missed because of an ECMWF data file name change. The reliability of satellite data delivery has declined significantly since the last maintenance period. In December, 2002 a change of satellite data provider became necessary and was undertaken (item (iii) below). The reliability of satellite data delivery is therefore expected to improve in 2003.

In addition to the routine maintenance action described above, the following specific maintenance tasks were requested by ESO. Details on the action taken for each task are presented in the meetings, reports or appendices indicated. These tasks were:

(i) Feasibility and requirements for extending ESO forecasts of cloud cover and PWV to Chajnantor. Oral report, presentation and discussion, July 16, 2001, Garching.
(ii) Analysis of discrepancies in Chajnantor 183 GHz radiometer data. (Erasmus, 2002)
(iii) Change of satellite data provider from CIRA to The Space Science and Engineering Center (SSEC), University of Wisconsin. (Appendix B)

A log of maintenance action taken over the contract period may be found in Appendix A.

3. Revision of the movement algorithm

In Erasmus and Maartens (2001), it was shown that forecast accuracy for cloud cover and, to a lesser extent, water vapour declines noticeably for forecast periods beyond 9 hours into the future. An examination of cloudy events in the period May 1999 to September 2001 showed that forecast inaccuracy at Paranal occurred during the summer months (December – March) when the active convective season east of the Andes is stronger than normal. Under these conditions easterly motion across the Andes occurs more frequently. The possibility of easterly motion is not allowed for in the movement algorithm used in the current (2^{nd}) version of the forecast programme.

As work progressed with revision of the movement algorithm it was noticed that when clouds move from the east, they may dissipate before reaching the observatory sites. Consideration of this phenomenon led to the development of a cloud persistence algorithm to be applied when cloud movement is from the east. Additionally, when considering how to improve cloud cover forecasts for La Silla it was observed that cloud may develop in-place as the air stream is lifted over the Andes. Such orographic enhancement of cloud cover would not be predictable by considering movement alone. Consequently, an algorithm was developed in an effort to facilitate the forecasting of such orographic cloud. These supplementary algorithms go beyond the scope of the original proposal but their consideration and

evaluation was considered necessary given the objective of improving forecast accuracy. In the verification of forecast accuracy (section 5), the upgrade is first evaluated in terms of the movement algorithm revision alone and then in conjunction with the cloud persistence and orographic cloud algorithms.

At Paranal in the *summer* months (December – March), cloud that forms north and east of Paranal typically moves eastwards (away from the site) in the prevailing westerlies. In the initial development of the forecast programme, since anomalous easterly motion was found to be a rare event, it was not incorporated in the movement algorithm of the forecast programme. However, during the summer of 2000-01, the South American Convergence Zone (SACZ) east of the Andes was more well developed than usual and positioned south of the latitude of Paranal on several occasions. This increased cloudiness over Paranal because, (i) the upper-tropospheric Amazon (Bolivian) high was stronger than normal and cloudy, moist air was circulated in a counter-clockwise spiral from the Amazon area over Paranal with greater frequency, and (ii) when the SACZ is positioned south of Paranal's latitude the circulation is such that cloud from convection developing east of Paranal may be transported westwards over the site. While this type of cloud movement may be anomalous, it is not unusual during La Niña conditions. Consideration was therefore given to improving the prediction of cloud under these conditions by revising the movement algorithm in the forecast programme.

In-place orographic cloud formation influences the occurrence and prediction of cloud in the *winter* months at La Silla. Orographic cloud is rare at Paranal because of its proximity to the coast and because of being further from the Cordillera than La Silla. Moisture levels in the middle and upper troposphere are enhanced in the winter months at the latitude of La Silla due to the northward migration of the South Pacific Anticyclone. In the current movement algorithm of the forecast programme the eastward movement of cloud and water vapour is well represented. However, when the upper tropospheric humidity (UTH) is elevated, cloud may form as the air is lifted (hence cooled) over the Andes. In the period examined (May 1999 to September 2001), of 14 such events, 12 occurred in the winter of 1999, 2 in the winter of 2000 and none in the winter of 2001. Since the winter of 1998 (El Niño) was excluded, the relationship between orographic cloud occurrence and ENSO is unclear, but it was definitely suppressed during the time La Niña conditions prevailed.

Erasmus and van Staden (2001), using satellite data over the period July 1993 – September 1999 found that, in the southern part of Northern Chile (La Silla, Tololo) during an El Niño, *winter-time* cloudiness is enhanced while in areas further north (Paranal, Chajnantor) *summer-time* cloudiness was enhanced during La Niña events. The effect is proportional to the magnitude of the ENSO event. This is consistent with the pattern of orographic cloud observed in the period May 1999 to September 2001.

3.1 The summer-time situation

It is apparent from the discussion above that the correct prediction of cloud movement in the summer months (December – March) requires that the movement algorithm incorporates movement of cloud from the east across the Andes, whether it occurs directly or in a spiralling manner around the Amazon high. In the Subtropics in the summer, pressure systems are barotropic (horizontal pressure and

temperature surfaces do not intersect). In these types of pressure systems, cloud movement is determined primarily by the wind rather than movement of the pressure field. The opposite is true for winter-time baroclinic pressure systems.

In general, in a barotropic atmosphere the horizontal pressure gradient is relatively small and winds are accordingly light. Locally, were thunderstorms or clusters of thunderstorms occur, the horizontal wind field may be much stronger but this is confined to the near surface layer (below the 850mb pressure level) and the upper Troposphere (~ 200mb). This is the case because such convective storms develop strong updraft circulations requiring inflow (convergence) near the surface and outflow (divergence) aloft. Between these levels of convergence and divergence, at about the 500mb pressure level, is found the mean level of non-divergence. At this level, the wind field is unaffected by local convection and is therefore representative of the persistent, steady component of horizontal air motion occurring over periods of several hours. In view of these facts, the u (west-east) and v (south-north) components of the wind at 500mb are used to define cloud and water vapour motion in the movement algorithm for the summer (defined as December 1 to March 15 inclusive). This is applied at Paranal and La Silla.

With a suitably accurate prediction of movement, most persistent cloud areas will be correctly forecast. In Northern Chile essentially all cloud moving from the ocean falls into the persistent category. When clouds were observed east of the site and cloud movement was subsequently towards the site, in several cases, the clouds dissipate by some amount before they reach the site. Sometimes complete dissipation occurred. This is consistent with the fact that the air west of the Andes is frequently much drier than air east of the Andes. Therefore, simply predicting the air motion correctly as being from the east, will lead to several false alarms in the cloud forecast. To address this problem, a “cloud persistence factor” (CPF) was computed when it was determined that the forecasted movement was from the east across the Andes and cloud is present. Movement “from the east” is defined as that situation where one or more of the forecast areas along the trajectory (most likely path) to the site are located east of the site.

From theoretical considerations and observational data (Pruppacher and Klett, 1980; Young, 1993) it is possible to quantify the fractional decrease in cloud particle mass for a given path length into air of different relative humidities. Since the upper tropospheric humidity and speed of the wind between the cloud and the site is known, it is therefore possible to determine cloud persistence. The likelihood of persistence is, in fact, very low. For a typical wind speed, cloud moving into an airmass with relative humidity less than 70% will survive only one hour. At 90% relative humidity survival is 3 hours. Essentially, the air has to be saturated or near saturation along the most likely path in order for cloud to survive passage across the Andes.

The cloud persistence factor (CPF) is computed for each forecast period if one or more forecast (satellite) areas are located east of the site and cloud is determined to be present in these areas.

Computation of the CPF:

(i) A forecast (satellite) area east of the site is defined as having cloud if the opaque cloud fraction is greater than 10%

(ii) UTHavg is computed for *all* forecast periods (areas). Pixels with opaque or transparent cloud are assigned a UTH value of 100%.
(iii) If UTHavg ≥ 70% then CPF = UTHavg/100 otherwise CPF = 0
(iv) Compute the Cumulative Cloud Persistence Factor (CumCPF) for all forecast periods. CumCPF is the product of the CPF's of the forecast periods up to and including a given forecast period. Hence CumCPF1 = CPF1, CumCPF2 = CPF1*CPF2, CumCPF3=CPF1*CPF2*CPF3, etc...
(v) For forecast areas *east* of the site with cloud the Opaque Cloud fraction is multiplied by CumCPF. This quantity is then added to the Transparent Cloud fraction to obtain the Adjusted Cloud fraction.

3.2 The winter-time situation

In Erasmus and Stanko (1997) it was shown that cloud movement associated with winter-time baroclinic wave cyclones and fronts is not simply related to the wind field. Rather, translation and development of the pressure field are the dominant controls for cloud movement in these weather systems. In the development of the movement algorithm currently employed in the forecast programme these factors were given due consideration. Following an examination of cloud events in the period May 1999 – September 2001 it was confirmed that the existing movement algorithm does accurately predict the motion of clouds from the Pacific Ocean over Paranal and La Silla in winter. For W-E motion the u-component of the 500mb wind is used and for N-S movement a quantity Vdev, proportional to the meridional component of the geopotential thickness change, is used (Erasmus and Maartens, 1999).

As noted in section 2, during some winters there is an increase in the occurrence of in-place orographic cloud formation at La Silla. This cloud is formed as moist air is lifted over the Andes in the prevailing westerly flow. This phenomenon is extremely rare at Paranal because it is located close to the coast and further from the Cordillera than La Silla. Thus the air stream is not subject to significant orographic lifting up-wind of the site. For this reason the orographic cloud prediction algorithm outlined below was only implemented for La Silla.

The aim of the algorithm is to predict the occurrence of orographic cloud by determining whether the air stream subjected to lifting and adiabatic cooling over the Andes will reach its dew point temperature above the site. This goal should be achievable since information on the moisture in middle and upper levels is available from the satellite UTH measurement and the ECMWF temperature and wind fields are dependable. The air stream considered is the flow in a layer extending from the 700mb level to the 400mb level perpendicular to the Andean Cordillera approximately at the latitude of the site. The critical quantity to determine is the amount of lift experienced by the air stream between the coast and the site (in this case, La Silla). If this quantity can be determined objectively then it is relatively straight forward to compute the amount of cooling experienced by the air stream and whether the dew point will be reached.

In the algorithm described below, a default value for the amount of lift experienced by the air stream is first derived from simple flow considerations (Part A.). The fractional height of the flow at 500mb (surface to 100mb) over the ocean is maintained inland to La Silla (Figure 1). The actual height of the flow at La Silla is computed and the difference between this height and the 500mb height over the

ocean is the amount of lift experienced by the flow. This is, in effect, the lift that would occur under neutral atmospheric stability. In the middle troposphere over Northern Chile the atmosphere is almost invariably stable. When orographic cloud forms in the middle and upper troposphere above La Silla the atmosphere is clearly stable since the cloud has a stratiform appearance.

When the atmosphere is stable (typical) the amount of lift experienced by the air stream will be less than the default. Under these conditions the potential temperature (θ) increases with height (z) (i.e. $d\theta/dz>0$) and the concept of critical streamlines may be applied. In Part B. of the algorithm described below, the methodology employed was based on the "winds on critical streamline surfaces" (WOCSS) concept as formulated by Ludwig *et al*. (1991) and applied by Erasmus (1993). Under stable conditions, air displaced upwards will be cooler than its surroundings and subjected to a downward force. Therefore, work is required to move a volume of air upwards from its equilibrium altitude. In other words the displaced air gains potential energy.

The restoring force experienced by the displaced air parcel is proportional to the temperature difference between the parcel and the environment. This may be expressed in terms of the displacement distance (δz) and the difference between the environmental (Γ) and dry adiabatic (Γ_d) lapse rates. The corresponding acceleration (force per unit mass) is then given by:

$$d^2z/dt^2 = (g/T)(\Gamma - \Gamma_d)\,\delta z = (g/T)\,\delta z\,(d\theta/dz)$$

The change in potential energy is obtained by integrating the above expression with respect to z over the displacement distance. The acquired potential energy (E) is therefore given by:

$$E = (g/2T)(\delta z)^2 (d\theta/dz)$$

Where g is the acceleration due to gravity, T is the average temperature of the layer and δz is the layer thickness.

In the environment described above, where the flow encounters an obstacle and is lifted, the kinetic energy of the flow ($^1/_2U^2$) is expended as potential energy is gained. The maximum gain of potential energy and hence the maximum lift possible would occur when:

$$(g/2T)(\delta z)^2 (d\theta/dz) = {}^1/_2U^2$$

Therefore, the maximum lift possible would be:

$$\delta z = U\,[(g/T)(d\theta/dz)]^{-1/2}$$

For the purpose of determining if orographic cloud will form the maximum lift is used. Next, it must be determined if the air stream is moist enough and undergoes sufficient cooling to reach dew point above La Silla. The 500mb temperature is used to compute the saturation mixing ratio (x_s) of the air before lifting. The mixing ratio (x) of the air before lifting is derived from the UTH as forecasted using the satellite data and x_s ($x = UTH.\ x_s$). After lifting x remains unchanged, but x_s is reduced since the air is cooler. The orographic cloud factor (OCF) is the ratio of the original mixing ratio to

the saturation mixing ratio after lifting and cooling. Theoretically, if OCF > 1 then the dew point has been reached. In practice OCF values larger than 1 are needed in order for orographic cloud to be present. This is understandable since cooling computations are based on maximum possible lift of an air parcel. In reality this does not apply since the conversion from kinetic to potential energy is not complete and entrainment of environmental air occurs (the lapse rate is not exactly dry adiabatic). A determination of the OCF values associated with orographic cloud was done by examining satellite data for the winter of 1999. It was found that orographic cloud does not occur when the OCF is lower than 2.0. When the OCF is in the range 2.0 to 3.0 orographic cloud always occurs but the amount of cloud is highly variable in spatial and/or temporal coverage. When the OCF exceeds 3.0 orographic cloud always occurs and is widespread and persistent.

Orographic cloud may be the only cloud present or may form in conjunction with other cloud moving in from the west. Therefore it is difficult to relate a range of OCF values with a particular level of cloud enhancement. For the purpose of the verification described in section 4, the Adjusted Cloud fraction was determined to be the Total Cloud fraction plus 25% if the OCF was between 2.0 and 3.0 or plus 50% if the OCF ≥ 3.0. If the resultant value was greater than 100% it was set equal to 100%. The exact manner in which the OCF may be used to change or supplement the forecast output is yet to be determined. Some suggestions are presented in section 6.

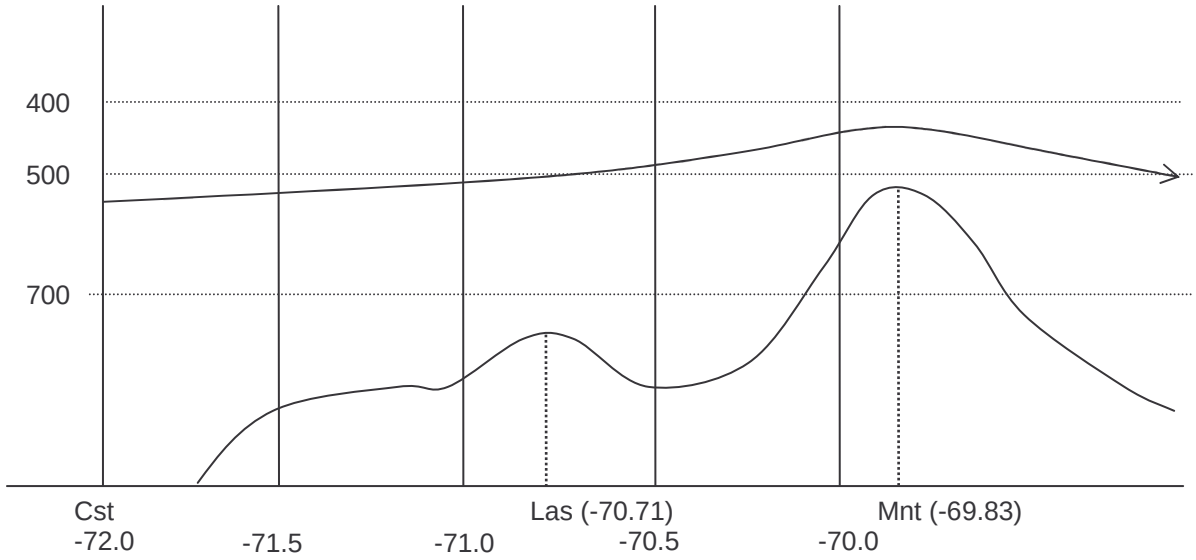

Figure 1. Schematic W-E cross-section at 29.5^{o}S showing orographic lifting of westerly flow over the Andes above La Silla Observatory (Las).

The orographic cloud algorithm is divided into three parts as follows:

A. At time-step 0 (the analysis time) compute the default value for the orographic lift experienced by the air stream between the ocean and La Silla:
   (i) Find the ECMWF grid-point at the latitude closest to the site (La Silla) to the west over the ocean (Cst). This is the grid point - 29.5, -72.0.

(ii) At this grid-point, using the geopotential heights (GPHgt) of standard pressure levels, compute HSig = GPHgt(500) / [GPHgt(100)-GPHgt(1000)]. HSig is the height of the flow at 500mb expressed as a fraction of the height of the troposphere. For this grid-point also define the actual height of this flow level, HgtFlowCst = GPHgt(500).

(iii) Define constant HgtLas = 2400m.

(iv) Then HgtFlowLas = [(GPHgt(100) - HgtLas)*HSig] + HgtLas is the height of the air stream as it traverses La Silla. Values for the grid point at -29.5, -70.5 are used.

(v) Lft2Las = HgtFlowLas-HgtFlowCst.

B. For each forecast time-step (i) compute the orographic lift experienced by the air stream based on the WOCSS concept (if this value is less than the default, it replaces the default in computations):

(i) For the Cst grid point, define constants:

U700cst = 700mb U at coastal grid point (m/s)
U500cst = 500mb U at coastal grid point (m/s)
U400cst = 400mb U at coastal grid point (m/s)
T700cst = 700mb Temp at coastal grid point (K)
T500cst = 500mb Temp at coastal grid point (K)
T400cst = 400mb Temp at coastal grid point (K)
Hgt700cst = 700mb geopotential height at coastal grid point (m)
Hgt500cst = 500mb geopotential height at coastal grid point (m)
Hgt400cst = 400mb geopotential height at coastal grid point (m)

(ii) For the 700-400mb layer, compute the mass-weighted average westerly flow velocity and temperature:

Ulayer = (4*U400 + 3*U500 + 5*U700)/12 (m/s)
Tlayer = (4*T400 + 3*T500 + 5*T700)/12 (K)

(iii) For the 700-400mb layer compute the rate of change of temperature with height:

DTDHgt = (T400cst – T700cst)/(Hgt400cst – Hgt700cst) (K/m)

(iv) Define the dry adiabatic lapse rate (a constant), DALR = -0.098 (K/m)

(v) Compute the geopotential, GeoPot = DTDHgt – DALR

(vi) Then Lft2LasStep = Ulayer / SQRT [gravity/Tlayer * GeoPot] (m), where gravity = 9.8 m/s^2.

(vii) If Lft2LasStep < Lft2las, then Lft2Las = Lft2LasStep.

C. For each forecast time-step (i), proceed to compute the relative humidity of the air stream after lifting and cooling and hence the probability of orographic cloud development

(i) The 500mb temperature (Tfp(i)) is used to compute the saturation mixing ratio (Xs(i)).

(ii) The forecasted UTH (i) is used to compute the mixing ratio as follows: X(i) = UTH (i). Xs(i).

(iii) The temperature of the air after lifting and cooling is computed, TfpCool (i) = Tfp (i) – DALR*Lft2Las.

(iv) The saturation mixing ratio after lifting and cooling (XsCool (i)) is computed using TfpCool(i).

(v) The orographic cloud factor, OCF (i) = X (i) / XsCool (i), is the relative humidity (as a fraction) after lifting and cooling.

(vi) A forecast of orographic cloud may be made as follows:

OCF (i) ≤ 2.0, Forecast = None
2.0 < OCF (i) < 3.0, Forecast = Possible
OCF (i) ≥ 3.0, Forecast = Probable

4. Verification of forecast accuracy

In the verification of forecast accuracy presented here the aim was to determine how application of the algorithms described in section 3 affect the accuracy of the UTH, PWV and cloud cover forecasts. The 2nd Version of the forecast programme (operational at the time of writing this report) and an Upgraded Version incorporating the algorithms described in section 3 were run on data for the period 1999-08-08 to 2001-10-11. Satellite imagery is typically available every three hours and, in conjunction with numerical meteorological forecast model data from ECMWF, these are used to produce forecasts for 3-hour periods extending 24 hours into the future. Over the period used in the verification 4039 forecast programme runs were executed producing approximately 27000 forecasts. Forecasted parameter values are synchronised to the mid-point time of the forecast period, thus 01:30UT, 04:30UT etc. The observed parameter value is obtained by averaging the measurements determined from the satellite images marking the start and end of the forecast period.

4.1 UTH and PWV

To test the accuracy of UTH and PWV forecasts the root mean square (RMS) difference between forecasted and observed values was computed. Any changes in the forecast accuracy for UTH and PWV between the 2nd and Upgraded versions of the forecast programme would be due to the revised movement algorithm. Additionally, it should be remembered that only the summer months (defined as 1 December to 15 March inclusive) are affected by the Upgrade. (see section 3).

Tables 1 and 2 show how the UTH and PWV forecast accuracy changes over 24 hours at the two sites. The results indicate that, overall, there is little or no change in forecasting accuracy for UTH and PWV between the 2nd Version and Upgraded Version of the forecast programme. There are, however, some subtle differences worth mentioning.

At both sites, for UTH, the Upgrade Version is consistently better, albeit very slightly, than the 2nd Version. This would not necessarily imply the same result for PWV since:

(i) in summer the PWV is determined largely by low-level moisture, and

(ii) the conversion from UTH to mixing ratio and PWV involves the use of a forecasted temperature from the ECMWF data and for motion east of the sites this parameter may be less predictable.

Regarding PWV, the results show that the Upgrade also performs slightly better than the 2nd Version at La Silla. At Paranal the 2nd and Upgrade versions perform similarly over the full 24-hours but the Upgrade Version is slightly worse for forecast time-steps beyond 18 hours ahead. This is most likely a computational effect, since, for

the last two forecast time-steps, fewer forecasts are generated by the 2nd Version than the Upgrade Version. It could also be a consequence of item (ii), above.

Table 1. Root mean square differences between forecasted and observed values of UTH (%) and PWV (mm) at Paranal for each 3-hourly forecast period to 24 hours ahead over the period 1999-08-08 to 2001-10-11.

Forecast Period	UTH (%) 2nd Version	UTH(%) Upgrade	PWV (mm) 2nd Version	PWV (mm) Upgrade
00-03hrs	2.4	2.4	0.38	0.37
03-06hrs	4.2	4.1	0.49	0.47
06-09hrs	5.5	5.4	0.59	0.59
09-12hrs	6.6	6.5	0.67	0.67
12-15hrs	7.3	7.3	0.74	0.75
15-18hrs	7.8	8.0	0.90	0.85
18-21hrs	8.5	8.5	0.84	0.90
21-24hrs	9.0	8.8	0.88	1.00

Table 2. Root mean square differences between forecasted and observed values of UTH (%) and PWV (mm) at La Silla for each 3-hourly forecast period to 24 hours over the period 1999-08-08 to 2001-10-11.

Forecast Period	UTH (%) 2nd Version	UTH(%) Upgrade	PWV (mm) 2nd Version	PWV (mm) Upgrade
00-03hrs	3.4	3.3	0.57	0.55
03-06hrs	5.6	5.5	0.73	0.72
06-09hrs	7.1	7.0	0.88	0.88
09-12hrs	8.2	8.2	1.02	1.03
12-15hrs	9.0	8.9	1.12	1.13
15-18hrs	9.9	9.6	1.25	1.23
18-21hrs	10.6	10.2	1.35	1.33
21-24hrs	10.8	10.0	1.47	1.40

4.2 Cloud cover

4.2.1 Total cloud cover

This quantity includes the fraction of transparent cirrus cloud as determined using the water vapour channel image (6.7µm) plus the fraction of opaque cloud detected either in the 6.7µm or 10.7µm image. Forecasted or observed amounts are expressed as the fraction of the sky covered by clouds at the analysis time or during each of the 3-hourly forecast periods. Four cloud cover (sky cover) categories, the same ones used in earlier comparisons (Erasmus and Maartens, 1999; 2001), were defined as follows:

Cloud Cover Category	% Total cloud	Fraction of sky that is clear
1. Clear	< 25	>0.75
2. Mostly Clear	25-50	0.50-0.75
3. Mostly Cloudy	50-75	0.25-0.50
4. Cloudy	>75	<0.25

In the part of the verification where accuracy was being assessed for cloudy days only, categories 2 and 3 were combined into one category. This was done in order to increase the number of counts in each category given the limited number of cloudy days. When forecasted and observed values are in the same category, a hit is counted. Neutral indicates values differ by one category and a miss by two or more categories.

In the verification of the cloud cover forecasts, the two aspects of the upgrade, namely, the movement algorithm revision and cloud cover adjustment (cloud persistence and orographic cloud), are evaluated separately. Firstly, the effect of the movement algorithm change *alone* was evaluated (Section 4.2.1.1). Secondly, both movement change and cloud adjustment were assessed (Section 4.2.1.2).

4.2.1.1 Evaluation of the movement algorithm revision

Tables 3 and 4 show the forecast accuracy for total cloud cover for forecast periods between zero and 24 hours and the 24-hour average at the two sites. The results show that, for clear and cloudy days, there is a slight improvement in forecast accuracy for the Upgrade Version at both sites. When evaluating the results it should be borne in mind that the movement algorithm revision affects only the summer months. In addition, while an important change to the movement algorithm allows for easterly motion this is a rare situation at Paranal (11.2%) and La Silla (4.2%).

Table 3. Percentage frequency of occurrence of total cloud cover forecasts classified as hit, neutral and miss at Paranal for each 3-hourly forecast period to 24 hours and the 24-hour average over the period 1999-08-08 to 2001-10-11. Clear and cloudy days are included.

Total Cloud	2nd Version			Upgrade (movement only)		
Forecast Period	%Hit	%Neut	%Miss	%Hit	%Neut	%Miss
00-03hrs	93.3	4.1	2.6	93.7	4.2	2.1
03-06hrs	91.6	3.9	4.5	92.2	3.7	4.1
06-09hrs	90.6	3.3	6.1	91.3	3.3	5.4
09-12hrs	89.7	3.1	7.1	90.5	2.9	6.6
12-15hrs	89.6	2.7	7.7	90.1	2.7	7.1
15-18hrs	89.3	2.4	8.4	89.9	2.8	7.3
18-21hrs	88.7	2.4	8.9	89.6	2.8	7.5
21-24hrs	87.9	2.6	9.4	89.7	3.1	7.2
0-24hrs Avg.	90.4	3.2	6.4	91.1	3.2	5.7

Table 4. Percentage frequency of occurrence of total cloud cover forecasts classified as hit, neutral and miss at La Silla for each 3-hourly forecast period to 24 hours and the 24-hour average over the period 1999-08-08 to 2001-10-11. Clear and cloudy days are included.

Total Cloud	2nd Version			Upgrade (movement only)		
Forecast Period	%Hit	%Neut	%Miss	%Hit	%Neut	%Miss
00-03hrs	88.0	7.4	4.6	88.0	7.6	4.5
03-06hrs	84.4	7.1	8.5	84.7	6.8	8.5
06-09hrs	82.1	6.8	11.1	82.3	6.5	11.2
09-12hrs	79.9	6.5	13.6	80.1	6.5	13.4
12-15hrs	78.8	6.7	14.5	79.4	6.4	14.2
15-18hrs	77.6	6.5	15.9	78.4	6.2	15.4
18-21hrs	76.2	6.3	17.5	77.7	6.0	16.3
21-24hrs	75.0	6.1	18.8	78.6	5.3	16.1
0-24hrs Avg.	81.1	6.8	12.1	81.6	6.5	11.9

Tables 5 and 6 show the verification results for cloudy days only. The improved performance of the Upgrade Version is more readily apparent, particularly at Paranal. The greater improvement at Paranal makes sense since easterly motion occurs more frequently at this site than it does at La Silla. The improvement in accuracy is particularly noticeable for forecast time-steps beyond 12 hours into the future. For these time-steps the hit rate has increase between 5% and 12%. Increasing the forecast accuracy for these later time-steps was one of the stated goals of the forecast programme upgrade described in this report.

Table 5. Percentage frequency of occurrence of total cloud cover forecasts classified as hit, neutral and miss at Paranal for each 3-hourly forecast period to 24 hours and the 24-hour average over the period 1999-08-08 to 2001-10-11. Only days observed to be cloudy are included.

Total Cloud	2nd Version			Upgrade (movement only)		
Forecast Period	%Hit	%Neut	%Miss	%Hit	%Neut	%Miss
00-03hrs	65.7	32.4	1.8	68.6	30.6	0.8
03-06hrs	53.1	39.6	7.2	56.8	37.2	6.1
06-09hrs	47.9	37.8	14.3	53.2	34.4	12.4
09-12hrs	43.8	36.7	19.5	49.3	33.6	17.1
12-15hrs	42.0	36.0	22.0	47.3	33.8	18.9
15-18hrs	41.3	34.2	24.5	45.7	31.9	22.4
18-21hrs	37.0	34.8	28.3	44.1	32.4	23.5
21-24hrs	37.5	31.9	30.6	51.0	25.2	23.8
0-24hrs Avg.	47.7	35.9	16.4	52.7	33.0	14.4

Table 6. Percentage frequency of occurrence of total cloud cover forecasts classified as hit, neutral and miss at La Silla for each 3-hourly forecast period to 24 hours and the 24-hour average over the period 1999-08-08 to 2001-10-11. Only days observed to be cloudy are included.

Total Cloud	2nd Version			Upgrade (movement only)		
Forecast Period	%Hit	%Neut	%Miss	%Hit	%Neut	%Miss
00-03hrs	63.3	34.0	2.8	63.6	33.6	2.8
03-06hrs	50.3	38.0	11.7	51.2	37.1	11.7
06-09hrs	42.8	38.0	19.2	43.4	37.4	19.2
09-12hrs	36.8	38.8	24.3	37.7	38.4	23.9
12-15hrs	33.6	37.3	29.1	35.2	37.1	27.8
15-18hrs	29.6	38.4	32.0	31.3	38.1	30.6
18-21hrs	28.3	36.4	35.3	30.5	35.8	33.7
21-24hrs	24.7	37.1	38.2	27.8	35.7	36.5
0-24hrs Avg.	41.1	37.3	21.6	42.2	36.7	21.1

4.2.1.2 Evaluation of the cloud adjustment algorithms

For the purposes of evaluating the effects of the cloud adjustment algorithms on cloud cover forecasts, summer conditions were evaluated at Paranal and winter conditions at La Silla. The forecasting accuracy of the Upgrade Version with and without cloud adjustment was compared. Cloud adjustment at Paranal includes cloud persistence, as described in section 3.1. At La Silla in winter, the adjusted cloud fraction was computed using the orographic cloud factor. As explained in section 3.2, 25% was added to the opaque cloud fraction if the OCF was between 1.25 and 2.5 and 50% was added if the OCF ≥ 2.5. The 25% increment represents a shift of one cloud cover category.

Tables 7 and 8 show the results for Paranal for all days (clear and cloudy) and cloud days respectively. Tables 9 and 10 present the corresponding results for La Silla.

Table 7. Percentage frequency of occurrence of total cloud cover forecasts classified as hit, neutral and miss at Paranal for each 3-hourly forecast period to 24 hours and the 24-hour average during the summers (1 December to 15 March) of 1999-2000 and 2000-2001. Clear and cloudy days are included.

Total Cloud	Upgrade			Upgrade with cloud adjustment		
Forecast Period	%Hit	%Neut	%Miss	%Hit	%Neut	%Miss
00-03hrs	94.4	4.0	1.6	94.4	4.0	1.6
03-06hrs	93.4	3.8	2.8	93.3	4.1	2.6
06-09hrs	92.7	4.1	3.2	93.1	3.8	3.0
09-12hrs	92.2	3.2	4.6	92.7	3.5	3.8
12-15hrs	91.2	3.9	4.8	91.7	4.3	3.9
15-18hrs	91.8	3.7	4.4	91.5	4.7	3.8
18-21hrs	91.4	3.7	4.9	90.6	5.0	4.4
21-24hrs	91.3	3.9	4.8	90.8	4.6	4.6
0-24hrs Avg.	92.4	3.8	3.8	92.4	4.2	3.4

Table 8. Percentage frequency of occurrence of total cloud cover forecasts classified as hit, neutral and miss at Paranal for each 3-hourly forecast period to 24 hours and the 24-hour average during the summers (1 December to 15 March) of 1999-2000 and 2000-2001. Only days observed to be cloudy are included.

Total Cloud	Upgrade			Upgrade with cloud adjustment		
Forecast Period	%Hit	%Neut	%Miss	%Hit	%Neut	%Miss
00-03hrs	75.5	24.5	0.0	75.5	24.5	0.0
03-06hrs	72.2	24.5	3.3	72.2	24.5	3.3
06-09hrs	71.0	24.5	4.6	71.0	24.5	4.6
09-12hrs	68.9	23.2	7.9	68.5	23.7	7.9
12-15hrs	66.4	24.5	9.1	66.0	24.9	9.1
15-18hrs	68.2	21.5	10.3	65.0	25.1	9.9
18-21hrs	65.5	23.2	11.3	60.1	29.1	10.8
21-24hrs	67.2	20.1	12.6	63.2	23.6	13.2
0-24hrs Avg.	69.5	23.4	7.1	68.0	24.9	7.0

For both clear and cloudy conditions the addition of cloud adjustment by cloud dissipation when cloud movement is from the east produces only the slightest improvement in forecast accuracy. The miss rate is marginally reduced. Consideration of days *observed* to be cloudy shows a slight decrease in accuracy when cloud adjustment is applied with a shift of some cases from the hit to the neutral category. However the miss rate is unaffected. Given the combination of results in Tables 7 and 8 it may be concluded that days *forecast* to be cloudy but *observed* as clear (false alarms) were reduced when the cloud adjustment algorithm was applied. This was confirmed to be the case. For the Upgrade Version without and with cloud adjustment there were, respectively, 1488 and 1482 cloudy forecasts during the period used for forecast verification. Of these, 217 were completely missed (clear conditions were observed) in the case of the upgrade without cloud adjustment while, with cloud adjustment, 177 cases fell into this category. This represents an 18.4% reduction in the false alarm rate. It was noteworthy that the maximum reduction in false alarm forecasts, from 78 to 57 (out of 401), occurred for the 9h-12h and 12h-15h forecasts.

Table 9. Percentage frequency of occurrence of total cloud cover forecasts classified as hit, neutral and miss at La Silla for each 3-hourly forecast period to 24 hours and the 24-hour average during the period 1999-08-08 to 2001-10-11. Clear and cloudy days for winter months are included.

Total Cloud	2nd Version and Upgrade			Upgrade with cloud adjustment		
Forecast Period	%Hit	%Neut	%Miss	%Hit	%Neut	%Miss
00-03hrs	84.3	9.7	6.0	84.7	10.2	5.1
03-06hrs	79.8	8.9	11.2	79.8	10.2	10.0
06-09hrs	76.8	8.5	14.7	75.9	10.0	14.1
09-12hrs	74.3	8.2	17.5	73.3	10.1	16.6
12-15hrs	72.9	8.4	18.6	71.7	10.0	18.4
15-18hrs	71.2	8.4	20.4	69.6	10.4	20.0
18-21hrs	69.1	8.4	22.4	67.9	10.2	21.9
21-24hrs	67.5	8.0	24.5	66.7	9.1	24.2
0-24hrs Avg.	75.7	8.6	15.7	74.9	10.1	15.0

Table 10. Percentage frequency of occurrence of total cloud cover forecasts classified as hit, neutral and miss at La Silla for each 3-hourly forecast period to 24 hours and the 24-hour average during the period 1999-08-08 to 2001-10-11. Only days observed to be cloudy in winter months are included.

Total Cloud	2nd Version and Upgrade			Upgrade with cloud adjustment		
Forecast Period	%Hit	%Neut	%Miss	%Hit	%Neut	%Miss
00-03hrs	62.6	34.3	3.1	65.7	32.7	1.6
03-06hrs	49.1	38.2	12.8	52.9	37.3	9.8
06-09hrs	40.9	38.2	20.9	42.4	41.1	16.5
09-12hrs	35.9	38.2	26.0	37.5	40.5	22.0
12-15hrs	33.0	37.1	29.9	34.3	39.4	26.3
15-18hrs	29.2	38.3	32.5	30.5	41.2	28.3
18-21hrs	27.9	36.5	35.7	29.8	38.4	31.8
21-24hrs	25.4	36.3	38.4	27.5	35.6	36.9
0-24hrs Avg.	40.3	37.2	22.5	42.4	38.4	19.1

In the comparison for La Silla the 2nd Version and Upgrade (without cloud adjustment) are identical since the revised movement algorithm affects only the summer months. Overall (clear and cloudy days), there is a slight decrease in accuracy when cloud adjustment is applied with a shift of some cases from the hit to the neutral category. However the miss rate is unaffected. When only days *observed* to be cloudy are considered, cloud adjustment improves forecast accuracy. The combination of results found for La Silla indicate that cloud adjustment using the orographic cloud factor enhances forecast accuracy when conditions are cloudy but also serves to increase the false alarm rate.

4.2.2 Transparent cirrus cloud cover

To provide consistency with verifications of forecast accuracy done in earlier studies an evaluation of the transparent cirrus cloud cover forecasts was also undertaken for the 2nd Version of the forecast programme and the Upgraded Version incorporating the movement algorithm change. The period 1999-08-08 to 2001-10-11 was used. In the verification, forecast periods during which more than 10% opaque cirrus was measured by the satellite were discarded. This was done so that this evaluation would indicate the skill in distinguishing between spectroscopic and photometric conditions on nights that are generally clear. Four categories of transparent cirrus cloud cover were defined as follows:

Cloud Cover Category	% Transparent Cirrus Cloud	Fraction of sky that is photometric under spectroscopic conditions
Clear	< 10	>0.90
Nearly Clear	10-25	0.75-0.90
Mostly Clear	25-50	0.50-0.75
Mostly Cloudy	>50	<0.50

Again, as in the case with total cloud, when forecasted and observed values are in the same category, a hit is counted. Neutral indicates values differ by one category and a miss by two or more categories. Note that the transparent cirrus cloud cover category thresholds have been selected to differentiate sky cover conditions more stringently when it is clear to mostly clear.

Tables 11 and 12 show that there is a very slight increase in forecast accuracy at both sites for the Upgrade Version compared to the 2nd Version. This is consistent with the results for total cloud. Similar to what is observed for total cloud, the increase in accuracy is greater for the later forecast periods.

Table 11. Percentage frequency of occurrence of transparent cloud cover forecasts classified as hit, neutral and miss at Paranal for each 3-hourly forecast period to 24 hours and the 24-hour average during the period 1999-08-08 to 2001-10-11. Days with more than 10% opaque cloud are excluded.

Total Cloud	2nd Version			Upgrade Version		
Forecast Period	%Hit	%Neut	%Miss	%Hit	%Neut	%Miss
00-03hrs	96.4	2.3	1.3	96.4	2.5	1.2
03-06hrs	95.6	1.9	2.5	95.4	2.2	2.4
06-09hrs	94.9	2.0	3.1	95.0	2.2	2.8
09-12hrs	94.6	2.0	3.5	94.9	2.0	3.1
12-15hrs	94.4	1.9	3.7	94.9	1.8	3.3
15-18hrs	93.6	2.2	4.1	94.5	2.0	3.5
18-21hrs	94.2	2.0	3.9	94.5	2.0	3.5
21-24hrs	93.5	2.5	4.1	94.0	2.0	4.0
0-24hrs Avg.	94.8	2.1	3.1	95.1	2.1	2.9

Table 12. Percentage frequency of occurrence of transparent cloud cover forecasts classified as hit, neutral and miss at La Silla for each 3-hourly forecast period to 24 hours and the 24-hour average during the period 1999-08-08 to 2001-10-11. Days with more than 10% opaque cloud are excluded.

Total Cloud	2nd Version			Upgrade Version		
Forecast Period	%Hit	%Neut	%Miss	%Hit	%Neut	%Miss
00-03hrs	91.7	5.2	3.1	91.7	5.1	3.2
03-06hrs	89.8	4.7	5.4	89.7	4.9	5.4
06-09hrs	88.8	3.9	7.2	88.5	4.2	7.3
09-12hrs	87.3	4.4	8.3	87.3	4.4	8.4
12-15hrs	87.0	3.9	9.1	87.3	4.0	8.7
15-18hrs	85.6	4.4	10.0	86.0	4.4	9.6
18-21hrs	84.9	3.9	11.2	85.7	3.9	10.4
21-24hrs	84.6	3.6	11.8	86.2	3.5	10.3
0-24hrs Avg.	88.0	4.3	7.7	88.1	4.4	7.5

5. A satellite-derived extinction parameter

5.1 Background

Satellite-derived indicators of atmospheric extinction (transparency) may be based on observations made by passive remote sensing at two infra-red wavelength bands. One channel is centred on 10.7µm in the infra-red window and the other on 6.7µm which is a water vapour absorption band. The satellite measures emission from the earth and atmosphere at these wavelengths. From this radiance measurement a brightness temperature can be derived as described below.

For GOES-8, radiance counts are 10-bits in length for the imager channels. The infra-red channel calibration consists of a bias scaling factor and a first order gain scaling factor. True radiance values are obtained using the equation:

$$R = (X - b)/m, \qquad (5.1)$$

where R is radiance (mW/[m^2.sr.cm^{-1}]) and X is the count value. The coefficients b and m are the scaling bias and the scaling gain, respectively. The brightness (or effective) temperature is then obtained by inverting the Planck function as follows:

$$T_{eff} = (c_2*nu)/\ln(1 + [c_1*nu^3]/R) \qquad (5.2)$$

where T_{eff} is effective temperature (K), "ln" stands for natural logarithm and nu (cm^{-1}) is the central wave number of the channel. The coefficients c_1 and c_2 are the two radiation constants and have values of $c_1 = 1.191066 \times 10^{-5}$ (mW.m^{-2}.sr^{-1}.cm^4) and c_2 = 1.438833 (cm.K). To convert effective temperature to actual temperature T(K), the following formula is used:

$$T = b*T_{eff} + a \qquad (5.3)$$

The constants a (K) and b depend on the observation channel. These are bias and gain adjustments that account for variations in the inverse Planck function across the spectral passband of the channel. The differences between the values of T and T_{eff} increase with decreasing temperature. They are usually of the order of 0.1 K and hence negligible for most calculations.

The 10.7µm channel brightness temperature, as computed using the above equations, is a measure of the surface (ground) temperature under clear conditions or of cloud top temperature when clouds are present. In combination with independent temperature measurements from rawinsondes or numerical forecast models these observations enable the detection of clouds and a determination of cloud height. Thus clear and cloudy (completely opaque) conditions may be discriminated.

Under clear conditions, the 6.7µm channel brightness temperature is quantitatively related to emissions from water vapour resident in the atmosphere between the 600mb and 300mb pressure levels. The Upper Tropospheric Humidity (UTH) is a measure of the relative humidity in this layer. For GOES data, Soden and Bretherton (1993, 1996) have derived a semi-empirical relationship between UTH and 6.7µm channel brightness temperature. The basic form of the relationship is:

$$UTH = [\exp(a + b*T) * \cos\theta] / p0 \qquad (5.4),$$

where θ is the satellite viewing zenith angle, a and b are the least squares fit slope and intercept of the regression line as defined by the empirical relationship and p0 is a normalized pressure variable.

$$p0 = p(T=240K)/ 300, \qquad (5.5)$$

where p (in mb) is the pressure level where the temperature (T) is 240K. The values for a and b are seasonally dependent and are obtained from a table listing their values for each month of the year. The factor p0 accounts for the lifting (lowering) of the weighting function peak (Figure 2) in warm (cold) airmasses.

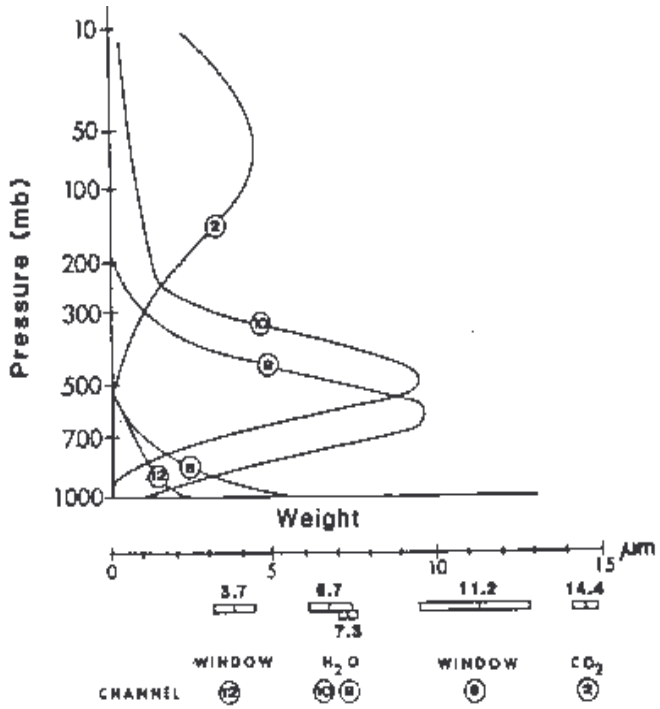

Figure 2. Weighting functions for IR observing channels (from Rao *et al.*, 1990)

From theoretical considerations the UTH is related to the growth of hydrometeors (liquid and solid water particles in suspension) and thus to atmospheric transparency. Atmospheric transparency at optical wavelengths is determined by the absorption and scattering of light on its path through the atmosphere (Figure 3). Absorption occurs largely at the molecular level but most atmospheric gases are not absorbent at optical wavelengths. In terms of day-to-day variability only water vapour has some impact on absorption. Extinction of light by scattering is much more significant and this is accomplished by smoke, dust, haze, cloud droplets and ice cloud particles. These particles have radii ranging in size from 0.1 μm to 1.0 μm and they produce Mie scattering of light. (Some scattering (Rayleigh) of light takes place at the molecular level but this does not contribute to extinction variations from day-to-day.)

In pristine environments associated with astronomical observatories it is reasonable to assume that smoke and, to a large extent, dust would have a small impact on extinction. Hydrometeors would therefore play the primary role in determining atmospheric transparency at optical wavelengths at these locations. This is

especially the case for day-to-day variability. Figures 4 and 5 show that the equilibrium hydrometeor size is controlled by the relative humidity of the air. In terms of scattering of light, the relative humidity range corresponding to the most significant range of particles sizes (0.1 µm to 1.0 µm) is between 60% and 100%.

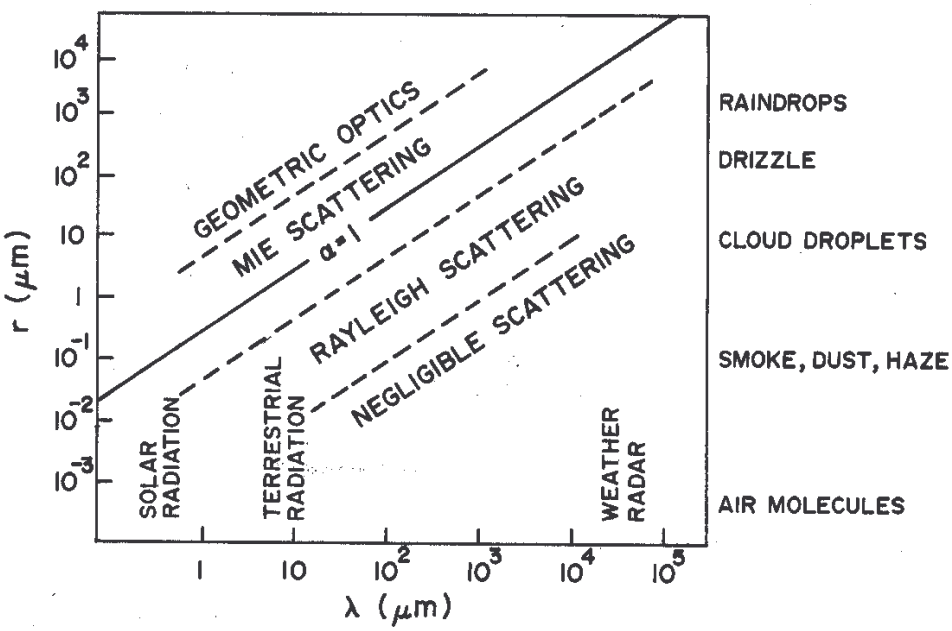

Figure 3. Size parameter (α) as a function of radiation wavelength and particle size. (From Wallace and Hobbs, 1977).

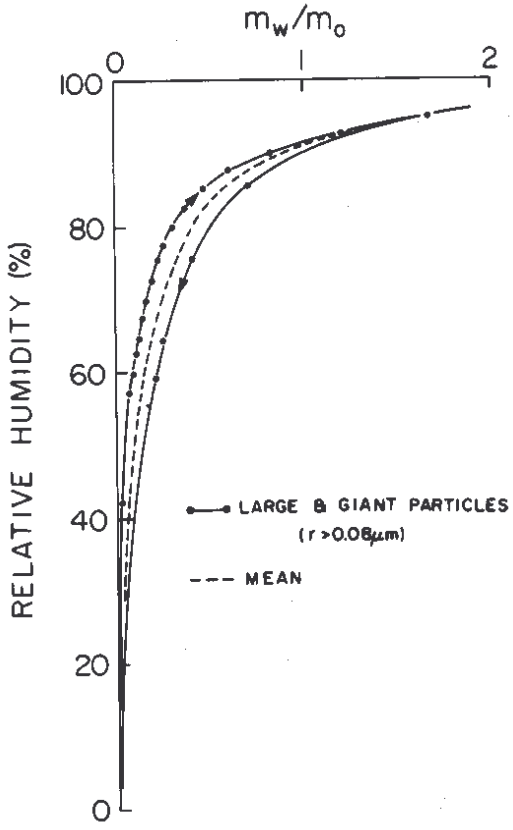

Figure 4. Equilibrium growth curve of natural aerosol deposit. Urban aerosol of continental origin. (From Winkler, 1967 as published in Pruppacher and Klett, 1980).

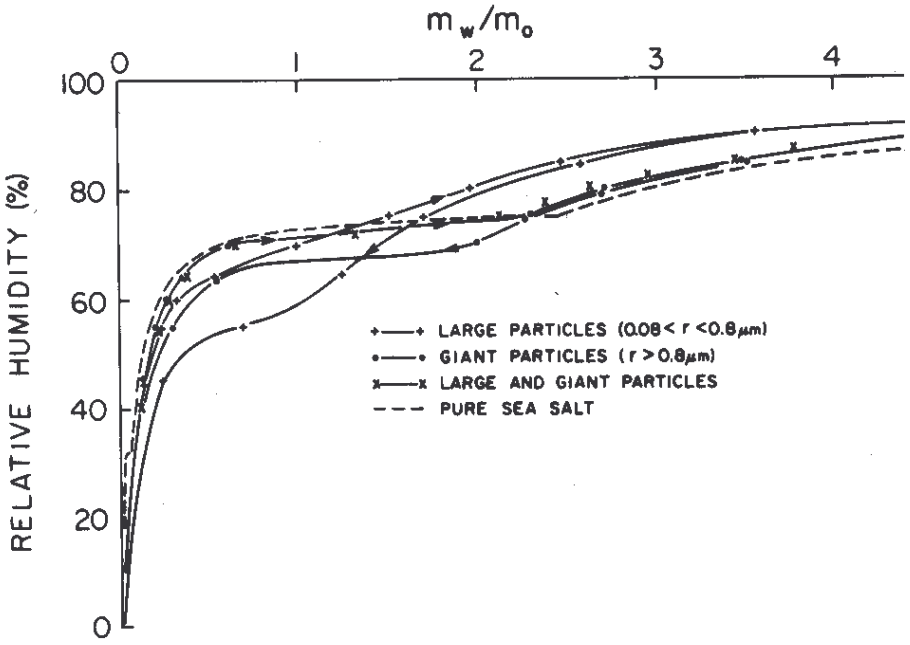

Figure 5. Equilibrium growth curve of natural aerosol deposit. Maritime aerosol. (From Winkler, 1967 as published in Pruppacher and Klett, 1980).

Figures 4 and 5 show that hydrometeor growth by condensation and deposition of water vapour on atmospheric aerosols (solid particles in suspension) starts when the relative humidity approaches 30%. The actual amount of water taken up and equilibrium particle size remains small until the relative humidity reaches 60% and thereafter increases considerably.

From the theoretical and observational considerations presented above it is reasonable to deduce that the satellite parameter UTH may be related to hydrometeor size and hence of atmospheric transparency. The added usefulness of establishing a link between UTH and transparency is that UTH is a highly predictable parameter thus providing the basis for transparency forecasts.

5.2 Previous work

In order to discriminate between clear conditions, thin transparent cirrus and opaque cirrus, Erasmus and Peterson (1996) visually compared cirrus clouds in water vapour channel and IR window channel images and deduced that the transition between clear conditions and transparent cirrus cloud occurred when the UTH reaches about 70%. When the UTH reached 150% the clouds were definitely opaque. (Since the relationship between UTH and T_{wv} is defined for clear conditions, when cloud particles reach a certain size the relationship breaks down and UTH values significantly higher than 100% may result. Additionally the more recent Sodden and Bretherton (1996) work produced an improved UTH calibration for GOES which subsequently led to a revision of these thresholds to 50% and 100% respectively).

In May 2000, an investigation was started (Erasmus and Sarazin, 2000) to relate satellite-derived water vapour and cloud cover parameters to atmospheric transparency as observed from the ground at Paranal and La Silla. Direct

measurements of atmospheric extinction have been made since early 1999 at Paranal and La Silla using the *Line Of Sight Sky Absorption Monitor* (LOSSAM). Using 9 months of observations for La Silla, a first attempt was made to relate the atmospheric extinction coefficient (E) as measured by LOSSAM to a transparency index (TI) derived from the satellite (Erasmus and Sarazin, 2002). TI was computed for a quasi-circular area of the satellite image centred on the site consisting of 45 pixels. The following criteria were used in the computation of TI: If all pixels are clear, TI=1.0. If all pixels are opaque then TI=0.0. If 10% or more of the pixels are opaque, TI is not applicable (n/a). If between 0% and 10% of the pixels are opaque, then TI is the average of the TI computed for the individual clear and transparent pixels, where:

(i) TI = 1.0 for clear pixels, and
(ii) TI = 1 - (UTHpixel - 50) / (150 - 50), for transparent pixels.

From observing experience in astronomy, a RMS atmospheric extinction lower than 0.01 magnitude corresponds to a perfectly photometric sky. In such conditions, the ratio of the absolute flux F_0 of a star to the actual flux F measured when observing through the atmosphere does not depend on the direction of observation but only on the zenith angle Ψ. The zenith dependency is characterised by an atmospheric extinction coefficient E for a given observing wavelength:

$$E = -2.5\cos\Psi\ [\mathrm{Log}(F)-\mathrm{Log}(F_0)].$$

A relationship between TI and E was defined for situations where the sky was not photometric but some type of astronomical observing, like spectroscopy, was still possible and where satellite-based forecasts of transparency would be of direct operational consequence. Based on satellite observations this included conditions with less than 10% sky coverage by opaque clouds. The LOSSAM RMS extinction measurements ranged from 0.01 to 0.1 magnitude. The corresponding extreme TI values were 1.0 and 0.3.

Meeting the above criteria, at La Silla observatory over the period January-October 2000, 486 pairs of observations were obtained with 406 (83.5%) perfectly photometric (E < 0.01) and 80 (16.5%) with E in the range 0.01-0.1. A parameter *Satrms* was defined by the regression relationship between E and Log(TI) for *non-photometric* conditions as follows:

$$Satrms = -0.3137\ [\log(TI) + 0.0182].$$

Applying this relationship to the full data set, *Satrms* is plotted versus E in Figure 6. Table 13 summarises the comparison.

It was found that the satellite-derived extinction parameter correctly discriminated between photometric and non-photometric conditions 86% (320/370) of the time. This preliminary work showed that the development of a satellite-derived extinction parameter that can discriminate between photometric and non-photometric conditions would likely prove to be successful.

Table 13. Satellite-derived atmospheric extinction (*Satrms*) and LOSSAM extinction (E) for photometric (E<0.01) and non-photometric (E>0.01) conditions at La Silla.

	Satellite	
LOSSAM	<0.01	>0.01
<0.01	287	45
>0.01	5	33

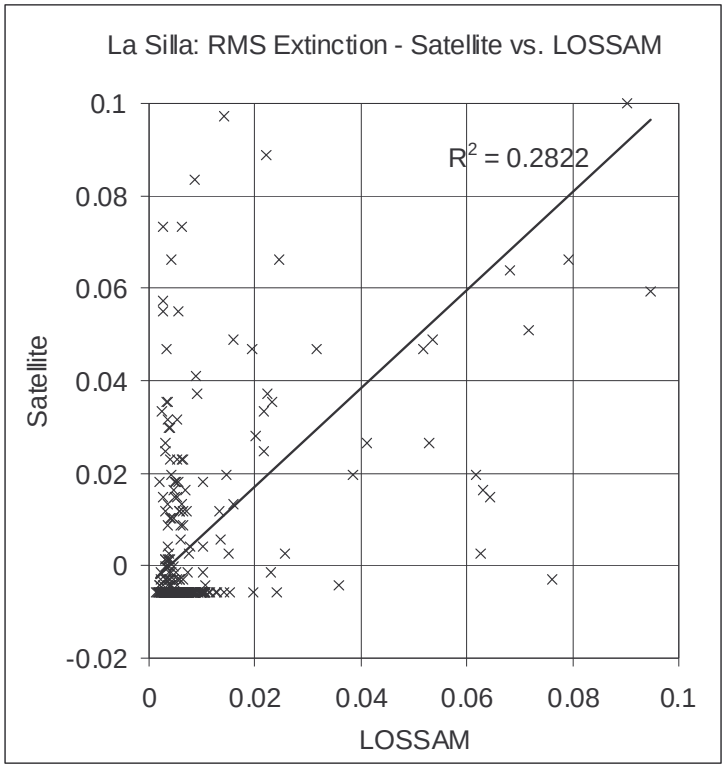

Figure 6. Satellite-derived atmospheric extinction (*Satrms*) versus LOSSAM extinction (E) for La Silla.

5.3 Continued development of a satellite-derived extinction parameter

Direct measurements of atmospheric extinction have now been made for three years at Paranal and La Silla using LOSSAM. This substantial database affords the opportunity to determine the validity of a satellite-derived indicator of atmospheric transparency over an extended period. In order to continue the work described in section 5.2 and apply the theory described in section 5.1, two years of LOSSAM and satellite data were analysed for both La Silla and Paranal observatories. Data were reduced for the period October 1999 to September 2001. The transparency index (TI) used in previous work was based on the UTH. For the analysis presented here, the UTH parameter was used directly since it is a continuous variable, the magnitude of which may be related theoretically to atmospheric extinction.

The LOSSAM extinction measurements were averaged over a 10-minute time window centred on the time when the satellite is scanning a particular site location. The satellite image time stamp corresponds to the starting time of a full earth-disk

scan which commences at 90^{o}N and proceeds line-by-line to 90^{o}S. A full earth scan takes 26 minutes. The satellite images used are every three hours starting at 02:45UT each day. The satellite pixel locations corresponding to Paranal and La Silla are scanned 18.43 min. and 19.38 min. respectively after the start of the satellite image scan. This is taken into account when synchronising the satellite and LOSSAM observations.

In the analysis presented here, the RMS extinction value marking the threshold between purely photometric and non-photometric conditions was adjusted from 0.01 to 0.02. This adjustment was made since experience gained observing oscillations in LOSSAM RMS extinction showed that when variability did not exceed 0.02 there was seldom a degeneration of observing quality to the point where opaque clouds prevailed. The lack of cloud under these conditions was confirmed in reports from observing astronomers (Sarazin, 2002).

Figure 7 shows scatter plots for Paranal and La Silla of LOSSAM RMS extinction versus UTH for the two year study period. The increase in extinction with UTH is clearly seen, particularly over the non-photometric range of LOSSAM extinction values. Also shown are the regression lines for the relationship between LOSSAM extinction and UTH for E > 0.02. The equations are:

(i) Paranal: Log(UTHavg) = 1.9575 + Log(RMSExt)*0.19429
(ii) La Silla: Log(UTHavg) = 2.1154 + Log(RMSExt)*0.30379

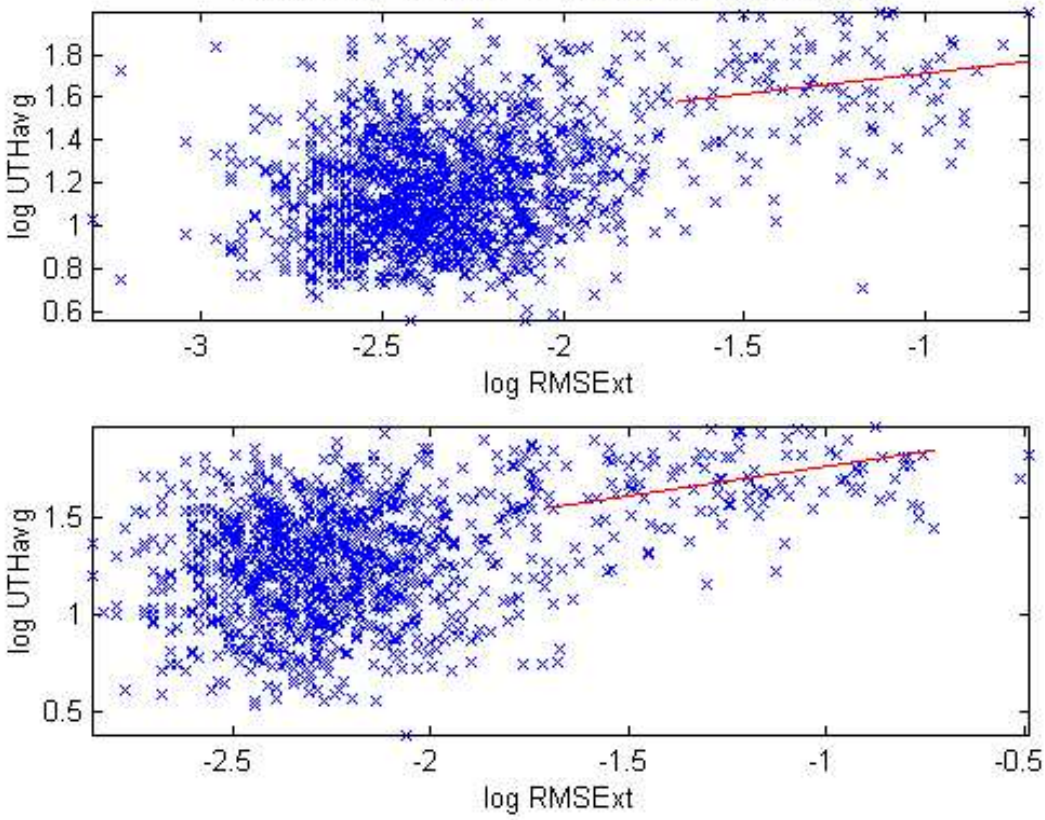

Figure 7. LOSSAM RMS extinction versus Satellite UTH for Paranal (top) and La Silla (bottom) showing regression relationships for non-photometric conditions.

Using the methodology described in section 5.2, a parameter *Satrms* was defined for Paranal and La Silla respectively using the regression relationships shown above. Thus,

(i) for Paranal: $Satrms = \exp_{10}[5.1469(\text{Log}(\text{UTHavg}) - 1.9575)]$, and

(ii) for La Silla: $Satrms = \exp_{10}[3.2917(\text{Log}(\text{UTHavg}) - 2.1154)]$,

where $\exp_{10}[\ ] = 10^{[\ ]}$ and Log is logarithm to the base 10.

At La Silla observatory over the period October 1999 – September 2001, 1165 pairs of observations were obtained with 1041 (89.4%) having E < 0.02 and 124 (10.6%) having E > 0.02. At Paranal, the total number of observations was 1424 pairs with 1324 (93%) having E < 0.02 and 100 (7%) having E > 0.02. *Satrms* was computed over the full range of extinction values (photometric and non-photometric) and is plotted versus the LOSSAM RMS extinction in Figure 8. Table 14 summarises the comparison.

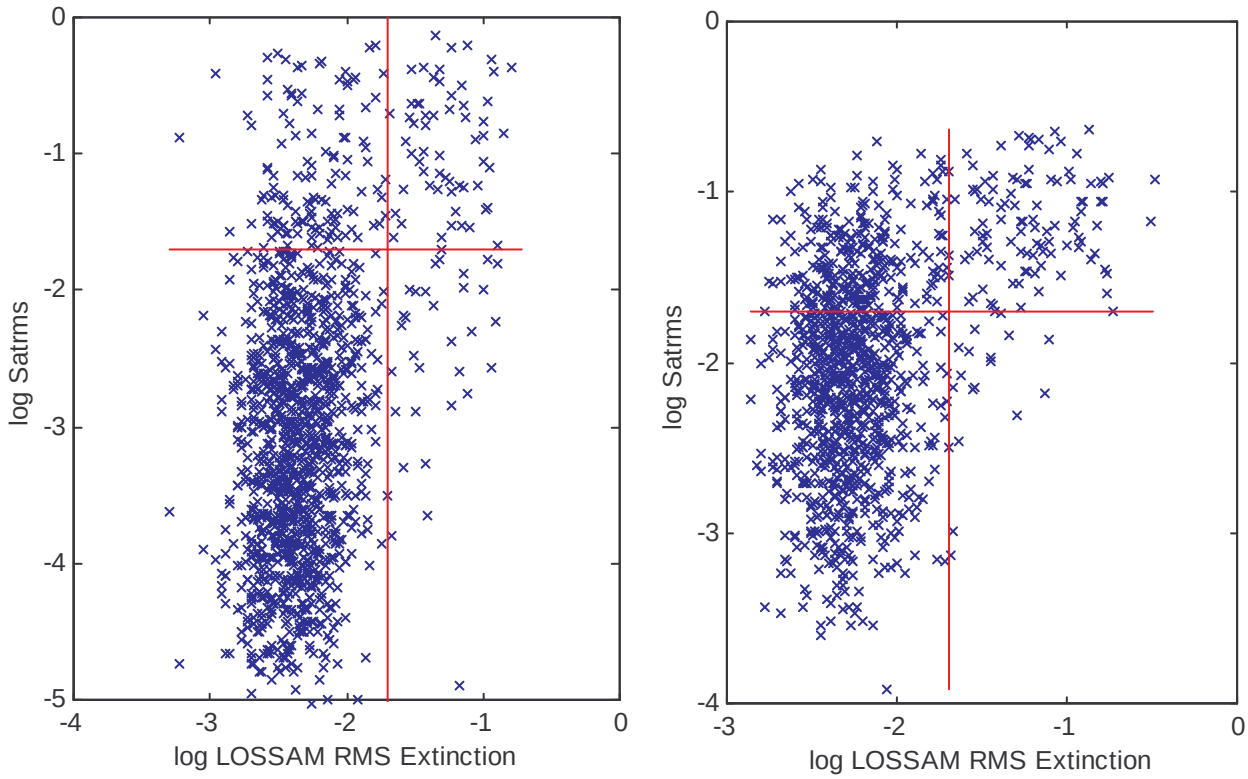

Figure 8. Measured LOSSAM extinction versus the satellite extinction parameter *Satrms* at Paranal (Left) and La Silla (right)

Table 14. Satellite-derived atmospheric extinction (*Satrms*) and LOSSAM extinction (E) for photometric (E<0.02) and non-photometric (E>0.02) conditions.

Paranal	Satellite	
LOSSAM	<0.02	>0.02
<0.02	1241 (87.2)	83 (5.8)
>0.02	39 (2.7)	61 (4.3)

La Silla	Satellite	
LOSSAM	<0.02	>0.02
<0.02	874 (75.0)	167 (14.3)
>0.02	32 (2.7)	92 (8.0)

From the above it may be concluded that if the satellite indicates conditions are photometric, observing quality is indeed photometric (97% of the time at Paranal and 96% of the time at La Silla). However, when the satellite indicates conditions are non-photometric the actual observing quality may be either photometric or non-photometric. Since photometric conditions occur a large fraction of the time the overall hit rate for agreement between the satellite and LOSSAM is 91.5% for Paranal and 83% for La Silla.

In terms of the potential for using the satellite extinction parameter in forecasting mode, it is clear that confidence in the forecast would be crucially dependent on whether the forecast is for conditions to be photometric or non-photometric. Photometric conditions can be predicted with great confidence but when the forecast is for conditions to be non-photometric there is uncertainty. Levels of confidence or uncertainty may be expressed as a probability using the forecasted UTH values on which the parameter *Satrms* is based.

Table 15 shows the percentage of time that observing conditions are respectively photometric or non-photometric for different ranges of UTH values.

Table 15. Number (first column) and percentage (second column) frequency of occurrence of photometric and non-photometric observing conditions for different ranges of UTH values.

Paranal	UTH (%)									
Extinction	< 30		30-50		50-80		> 80		> 80+cloud	
< 0.02	1166	98	116	78	41	58	1	9	1	1
≥ 0.02	27	2	33	22	30	42	10	91	109	99
La Silla	UTH (%)									
Extinction	< 30		30-50		50-80		> 80		> 80+cloud	
< 0.02	787	97	200	81	53	55	1	9	1	0
≥ 0.02	24	3	47	19	43	45	10	91	269	100

For UTH values below 50% predictability would be high using the satellite parameter *Satrms*. For UTH>80% predictability is again high (better than 90%). When cloudy events are included in the counts for non-photometric observing conditions (E>0.02), as shown by figures in parentheses, predictability is virtually 100%. Therefore, it is only in the range of UTH values between 50% and 80% that the forecast would be indeterminate. This range of UTH values is observed only 4.7% of the time at Paranal and 6.7% of the time at La Silla. Therefore a forecast of atmospheric extinction based on the satellite parameter *Satrms* would be useful a large fraction of the time.

The question why the satellite sometimes indicates conditions are non-photometric when they are photometric was investigated further. The satellite parameter *Satrms* is based on the relationship between the UTH and extinction (hydrometeor size and number). This implies that there are times that the UTH is relatively high but extinction remains low. From Figures 4 and 5 it can be seen that for condensation nuclei from a marine source compared to a continental source, the same UTH supports larger particle growth in the case of maritime air. Possibly, then, lower extinction would result if air flow is from the continent rather than the ocean. The data were re-plotted so as to discriminate between conditions where the u (westerly) component of the wind is greater than 5 m/s, between -5 m/s and 5 m/s and less than -5 m/s. The plots are shown in Figure 9.

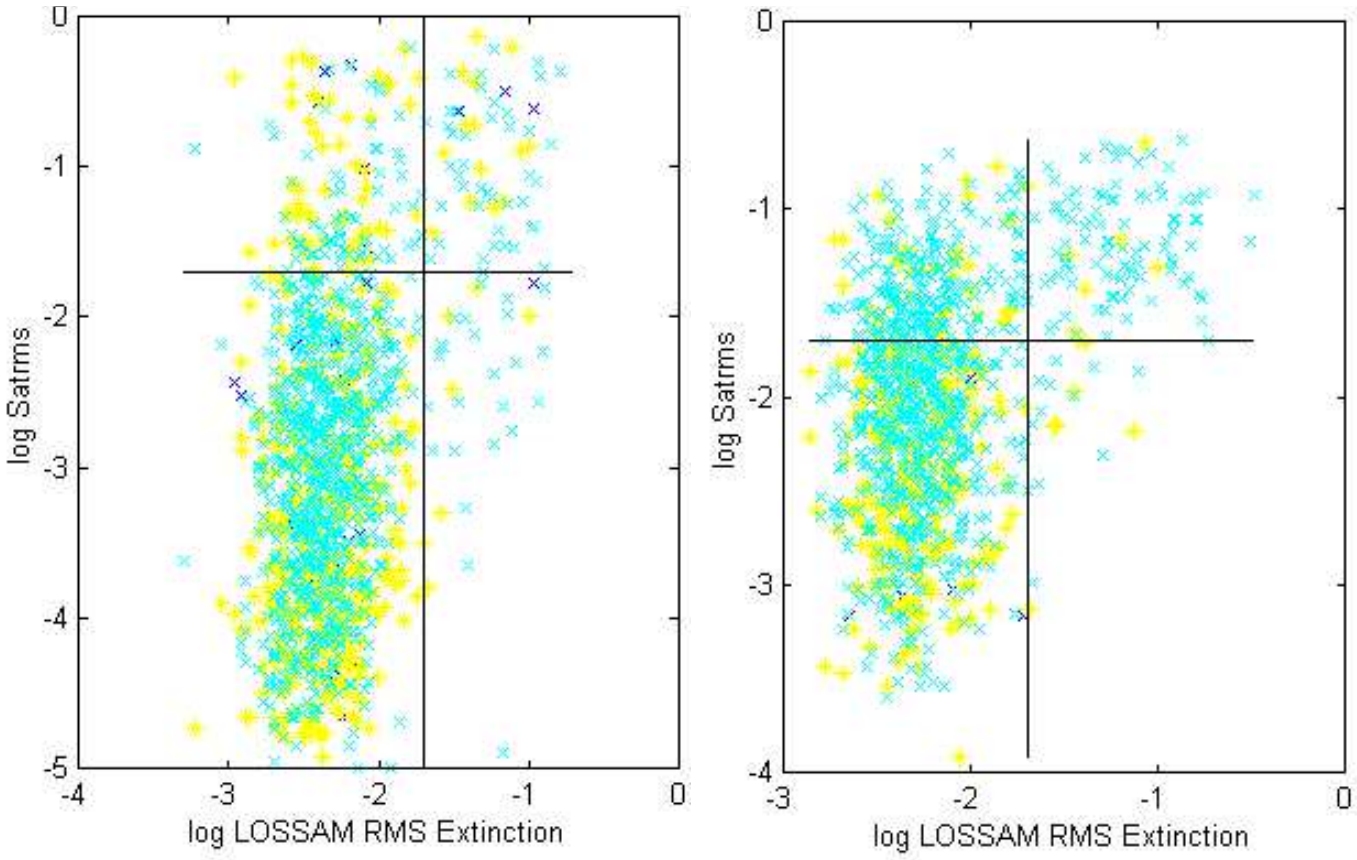

Figure 9. Measured LOSSAM extinction versus the satellite extinction parameter *Satrms* at Paranal (Left) and La Silla (right) plotted according to magnitude of the u (westerly) wind component. Blue (dark x): < -5 m/s, Yellow (*): -5 m/s to 5 m/s, Cyan (light x): > 5 m/s.

In the plots it can be seen that there is no clear stratification of *Satrms* values on the basis of wind direction when the observed extinction is in the non-photometric range. So the hypothesis that the airmass source (maritime or continental) effects extinction is shown not to be valid.

6. Suggestions and recommendations regarding forecast products

This report describes several revisions to the forecast programme that is currently being used to provide operational forecasts of water vapour and cloud cover to ESO observatories at Paranal and La Silla. The impacts of these revisions on forecast accuracy have been evaluated. Additionally, a satellite-derived extinction parameter has been developed and tested in terms of its ability to discriminate between photometric and non-photometric conditions. It now remains to be decided which of these changes and additions will be implemented operationally and in what manner.

The primary component of the upgrade involved revision *of the movement algorithm*. For both sites application of the revised movement algorithm resulted in an improvement in forecast accuracy. It is therefore recommended that this revision be implemented in the next upgrade of the operational forecast programme. In terms of the forecast products, no change would be necessary since this component of the upgrade works in conjunction with existing output parameters and forecast products.

Secondary or supplementary components of the upgrade include two cloud adjustment algorithms. The first of these is the *cloud persistence algorithm* which applies at Paranal and La Silla when cloud moves from the east in the summer. A cloud persistence factor (CPF) was used to adjust the opaque cloud fraction which was then added to the transparent cloud fraction to give an Adjusted Cloud fraction. It was found that cloud adjustment using the (CPF) improves forecast accuracy at Paranal and La Silla. It is suggested that a column be added to the text forecast products listing the Adjusted Cloud fraction. If no adjustment is made, the Total Cloud fraction would be repeated in the Adjusted Cloud column. Alternatively, information on cloud adjustment could be encoded symbolically in the Adjusted Cloud column using, for example, a “-“ to indicate that a moderate reduction in the Total Cloud fraction is expected or “--“ to show that a large reduction in the Total Cloud fraction is expected. In the latter case the Total Cloud fraction would not necessarily be repeated.

The *orographic cloud algorithm* aims to improve prediction of cloud cover at La Silla in the winter. For verification purposes, the orographic cloud factor (OCF) was converted into a cloud fraction which was then added to the Total Cloud fraction to give the Adjusted Cloud fraction. The thresholds applied were as follows:

(i) OCF < 2.0: add nothing
(ii) 2.0 < OCF < 3.0: add 25%
(iii) OCF ≥ 3.0: add 50%

It was found that the Adjusted Cloud fraction thus computed resulted in an improvement in forecast accuracy under cloudy conditions but when it was clear the frequency of false alarms (cloudy forecasts) increased. Given this result, the explicit computation of an Adjusted Cloud fraction for La Silla in winter is not recommended. However the information provided by the orographic cloud factor is clearly useful. Therefore a probability type forecast is suggested as follows:

(i) OCF < 2.0: no orographic cloud
(ii) 2.0 < OCF < 3.0: orographic cloud possible (+)
(iii) OCF ≥ 3.0: orographic cloud probable (++)

The "+" or "++" symbol would be written in the Adjusted Cloud column with or without the Total Cloud amount.

A comparison between the satellite-derived extinction parameter, *Satrms*, and extinction measurements made on the ground at Paranal and La Silla showed that *Satrms* is a reliable indicator of photometric conditions. However when the satellite indicated conditions are non-photometric, actual observing quality could be photometric or non-photometric. In the latter case, a useful probabilistic forecast could nevertheless be made. Based on these findings a suggested application of the satellite extinction parameter in forecasting mode would be as follows:

(i) *Satrms* < 0.02. Forecast: Probability of photometric conditions > 90%
(ii) *Satrms* ≥ 0.02 and UTH > 80%. Forecast: Probability of non-photometric conditions > 90%
(iii) Neither (i) nor (ii). Forecast: Observing conditions indeterminate

7. References

Erasmus, D.A., 1993: Objective simulation of topographically modified boundary layer winds in areas of complex terrain along the South African coast. Workshop manual. August 3, 1993, Department of Oceanography, University of Cape Town. 40pp.

Erasmus, D.A., 2002: An Analysis of Cloud Cover and Water Vapor for the ALMA Project: A Comparison Between Chajnantor (Chile), Chalviri (Bolivia) and Five Sites in Argentina using Satellite Data and a Verification of Satellite PWV measurements. The Atacama Large Millimetre Array Project, European Southern Observatories. Final Report under contract number 66814/ODG/02/6419/GWI/LET.

Erasmus, D.A. and D.S. Maartens, 1999: Operational Forecasts Of Cirrus Cloud Cover And Water Vapour Above Paranal And La Silla Observatories. European Southern Observatories. Report under contract number 52538/VPS/97/9480/HWE.

Erasmus, D.A. and D.S. Maartens, 2001: Maintenance, Upgrade and Verification of Operational Forecasts of Cloud Cover and Water Vapour above Paranal and La Silla Observatories. European Southern Observatories Report under contract number 58311/ODG/99/8362/GWI/LET.

Erasmus, D.A. and M. Sarazin, 2000: Forecasting Precipitable Water Vapour and Cirrus Cloud Cover For Astronomical Observatories: Satellite image processing guided by synoptic model dissemination data. SPIE Conference on Image and Signal Processing for Remote Sensing IV. Paper SPIE-4168, Barcelona. 25-29 September, 2000.

Erasmus, D.A. and M. Sarazin, 2002: Utilising Satellite Data For Evaluation and Forecasting Applications At Astronomical Sites. IAU SITE2000 Conference: Astronomical Site Evaluation in the Visible and Radio Range. Marrakech, Morocco, 13-17 November, 2000. Proceedings. In Press.

Erasmus, D.A. and C.A. van Staden, 2001: A Satellite Survey of Water Vapour and Cloud Cover in Northern Chile. Final Report. Cerro-Tololo Inter-American Observatory.

Erasmus, D.A. and P.R. Stanko, 1997: Feasibility Study and Development of Software Computer Code for Cloud Cover and Water Vapour Forecasts: Phase II - Parameter Definitions and Requirements for an Operational System. European Southern Observatories, Report No. VLT-TRE-ERA-17440-1039.

Ludwig, F.L., J.M. Livingston and R.M. Endlich, 1991: Use of Mass Conservation and Critical Dividing Streamline Concepts for Efficient Objective Analysis of Winds in Complex Terrain. *J. Appl. Meteor*., 30, 1490-1499.

Pruppacher, H.R. and J.D. Klett, 1980: Microphysics of Clouds and Precipitation. Reidel, Dordrecht, 714pp.

Rao, P.K., S.J. Holmes, R.K. Anderson, J.S. Winston and P.E. Lehr, Eds., 1990: *Weather Satellites: Systems, Data and Environmental Applications*. American Meteorological Society, Boston, 503pp.

Soden, B.J., and F.P. Bretherton, 1993: Upper tropospheric relative humidity from the GOES 6.7μm channel: Method and climatology for July 1987. *J. Geophys. Res.* 96, 16669-16688.

Soden, B.J., and F.P. Bretherton, 1996: Interpretation of TOVS water vapor radiances in terms of layer-average relative humidities: Method and climatology for the upper, middle and lower troposphere. *J. Geophys. Res.* 101, 9333-9343.

Wallace, J.M. and P.V. Hobbs, 1977: *Atmospheric Science: An Introductory Survey*. Academic Press, New York, 467pp.

Winkler, 1967: Diploma Thesis, Meteorological Institute, University of Mainz.

APPENDIX A – MAINTENANCE ACTION LOG

2001.7.16-17
Report, Presentation and Discussion: "Feasibility and Requirements for Extending ESO forecasts to Chajnantor"

2001.7.~12
Power failure at CIRA. Some images not received.

2001.8.5
Dates on Outlook files. Problem investigated. Intermittent.

2001.8.20
Problems with satellite data on CIRA server (also, days prior). Communicated to CIRA

2001.9.20
ESO can not logon to CIRA server. Data not downloaded. Some forecasts missed.

2001.10.3
c03 file name change. Fix sent and installed.

2002.01.08-
Change to name of ECMWF data files

2002.04.26
Satellite data delivery interrupted. Payment issues between ESO and CIRA

2002.08.12
Satellite data missing from CIRA server. Contact Dean and McClurg to restore data. Data restored next day. Some data missing. requested recovery.

2002.08.14
Notification of switch from GOES-8 to GOES-12. Expected to take place by April 2003. Change in resolution for 6.7 micron. First assessment of changes required.

2002.11.26
Discrepancies detected in Chajnantor radiometer PWV data. Likely impact on forecasts of PWV at Chajnantor. Analysis requested by ESO.

2002.12.05-27
Notification of cancellation of satellite data delivery from CIRA. Action to setup satellite data delivery from SSEC. Resolution of data and file format matters. Creation, delivery and implementation of software patch for ESO forecast programme to run on satellite data from new data provider.

APPENDIX B – CHANGE OF SATELLITE DATA PROVIDER

Appendix B of Erasmus and Maartens (2001) contains a report on the results of an investigation into GOES satellite data providers. This investigation was motivated by the fact that some aspects of the service of the data provider at that time (CIRA) were not satisfactory. In addition, it was considered prudent to determine the availability of a suitable alternative data provider. The report identified The Space Science and Engineering Center (SSEC) at the University of Wisconsin as such an alternative satellite data provider. At that time, preliminary correspondence regarding data delivery and prices was entered into with the Manager of SSEC, Ms. Dee Wade.

This investigation has proven to be fortuitous, since, in early December 2002, ESO was advised by CIRA that delivery of the satellite data needed to produce the operational forecasts would cease at the end of 2002. Given the very short notice of cancellation of data delivery by CIRA, it was doubtful whether data acquisition could be resumed in time for the forecasts to continue uninterrupted. Communication with SSEC was re-established and rapid progress was made towards initiating data delivery from the new provider. While contractual matters were being handled between ESO and SSEC, data and file format concerns were being resolved between the proposal author and SSEC. Remarkably, data delivery in the required format was in place by December 26, 2002. A software patch needed to run the forecast programme was supplied to ESO on December 27, 2002 and the ESO forecasts were being produced on December 30, 2002 using the satellite data from the new data provider.